Journal of Molecular Graphics and Modelling 42 (2013) 120–128

Contents lists available at SciVerse ScienceDirect

Journal of Molecular Graphics and Modelling

journal homepage: www.elsevier.com/locate/JMGM

Theoretical study on optical and electronic properties of bipolar molecules with 1,8-naphthalimide and triphenylamine moieties as organic light-emitting materials

Ruifa Jin[a,*], Shanshan Tang[b]

[a] College of Chemistry and Chemical Engineering, Chifeng University, Chifeng 024000, China
[b] College of Resource and Environmental Science, Jilin Agricultural University, Changchun 130118, China

ARTICLE INFO

Article history:
Received 10 October 2012
Received in revised form 30 March 2013
Accepted 1 April 2013
Available online 9 April 2013

Keywords:
Bipolar molecule
Optical and electronic properties
Charge transport property
Light-emitting materials
Organic light-emitting diodes (OLEDs)

ABSTRACT

A series of D–π–A bipolar molecules with triphenylamine (TPA) fragments as donors, 1,8-naphthalimide (NI) fragments as acceptors, and different π-conjugated bridges (CB) as π-conjugated bridges have been designed to explore their optical, electronic, and charge transport properties as charge transport and luminescent materials for organic light-emitting diodes (OLEDs). The frontier molecular orbitals (FMOs), natural population analysis (NPA), and local density of states analysis have turned out that the vertical electronic transitions of absorption and emission are characterized as intramolecular charge transfer (ICT). The calculated results show that their optical and electronic properties are affected by the π-conjugated bridges in bipolar molecules. The electron-donating (-withdrawing) π-conjugated bridges serve as donors (acceptors) for the compounds under investigation. Our results suggest that these bipolar molecules are expected to be promising candidates for holes transport and luminescent materials for OLEDs. The results presented show that varying the π-conjugated bridges of bipolar molecules is a highly promising approach to develop this series of materials for OLEDs applications.

1. Introduction

The development of organic light-emitting diodes (OLEDs) has received a significant amount of attention in recent years due to their potential applications in the next-generation full-color flat-panel displays [1–8]. The organic electroluminescent devices have shown several advantages over inorganic ones, for example, light weight, potentially low cost, capability of thin-film, large-area, flexible device fabrication, and wide selection of emission colors via molecular design of organic materials. The main obstacle to the application of OLEDs is still their lower efficiency. The key to increase the efficiency of OLEDs is to balance the charge carrier transport. It is therefore necessary to design and synthesize multifunctional OLEDs materials, which are capable of transporting charge in addition to functionalizing as efficient emitters with excellent performance [9,10]. A number of studies demonstrate the interplay between theory and experiment, which is capable of providing useful insights to the understanding of the nature of molecules [11–13]. Among the various kinds of OLEDs emitters, 1,8-naphthalimide derivatives have attracted much attention owing to their good optical, thermal and chemical stabilities, as well as high photoluminescence quantum efficiency [14–16]. The imide nitrogen makes 1,8-naphthalimides easy to functionalize [17]. Furthermore, it has been reported that naphthalimide derivatives generally have high electron affinity due to the existence of an electron-deficient center [18–20] and should display good electron-transporting or hole-blocking capabilities that are appropriate for balanced carrier injection in OLEDs. On the other hand, triphenylamine and its derivatives have been typically used for OLEDs as hole transporting materials and blue light emission materials that take advantage of their excellent solubility, good stability, and high photoluminescent efficiency [21–23]. The substitution of triphenylamine at the 4-position of naphthalene-derived imides may be a good method to develop novel light-emitting materials with the balance of electron- and hole-transporting. Recently, a bipolar molecule containing both donor (triphenylamine) and acceptor (1,8-naphthalimide) moieties, 4-(di(4-methoxyphenyl)amine)benzaldehyde N-(2-ethylhexyl)-1,8-naphthalimide hydrazone, and its derivatives have been reported. They shown good optical and hole transporting properties [24].

Herein we report the investigation of both charge transporting and optical properties from theoretical point of view for this donor–π–acceptor (D–π–A) bipolar molecules system. Further in-depth interpretations of the available experimental electronic and spectroscopic characteristics have been discussed by the investigation of the optical and electronic properties of the derivatives.

* Corresponding author. Tel.: +86 0476 8300370; fax: +86 0476 8300370.
E-mail address: Ruifajin@163.com (R. Jin).

1093-3263/$ – see front matter © 2013 Elsevier Inc. All rights reserved.
http://dx.doi.org/10.1016/j.jmgm.2013.04.001

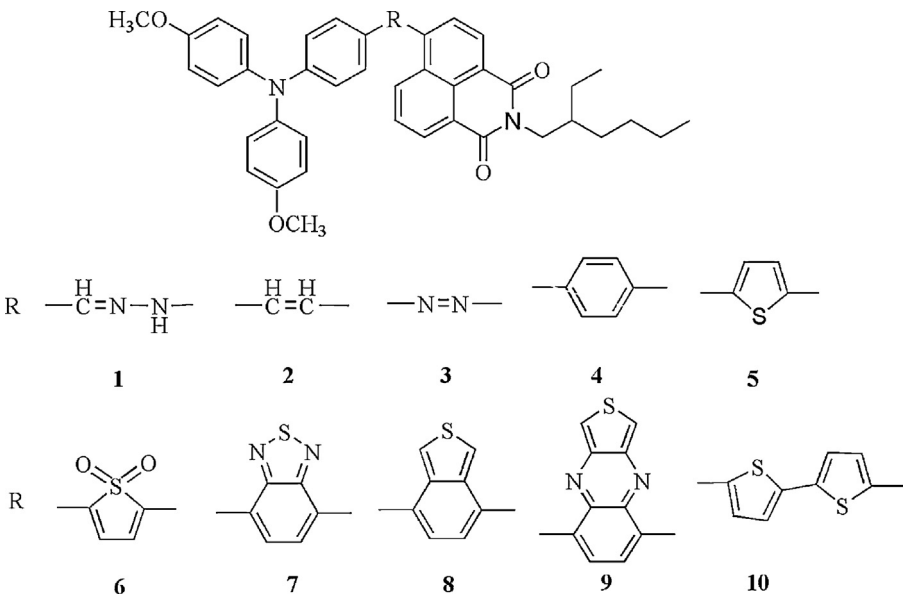

Fig. 1. Sketch map of the structures of **1**–**10**.

Furthermore, quantum-chemical studies of the substitution effect on the electronic and optical properties of the derivatives are thereby called for designing novel functional materials. To investigate the substituent effect, ten D–π–A bipolar molecules (**1**–**10**) with triphenylamine (TPA) fragments as donors and 1,8-naphthalimide (NI) fragments as acceptors, as shown in Fig. 1, have been designed by introducing different π-conjugated bridges (CB). The optical and electronic properties of these derivatives are predicted to provide a demonstration for the rational design of new candidates for luminescent and charge transport materials for OLEDs.

2. Computational methods

All calculations have been performed using Gaussian 09 code [25]. The unphysical long-range asymptote of the exchange part of popular functionals, e.g., B3LYP makes them unsuitable for calculations of excited states having a large charge-transfer (CT) component [26,27]. The systems of our current interest contain π-center with electron donors and acceptors on the terminal sites of the conjugated backbone and have a direct relationship with the charge transfer interactions in the excited state. Hence, the use of standard xc-functionals may not be appropriate. In the present work, we have used both B3LYP and the Coulomb attenuated method hybrid exchange correlation-functional (CAMB3LYP) [28], where the exchange part is separated into short- and long-range according to the following formula:

$$\frac{1}{r_{12}} = \frac{1-[\alpha+\beta\cdot erf(\mu\cdot r_{12})]}{r_{12}} + \frac{\alpha+\beta\cdot erf(\mu\cdot r_{12})}{r_{12}}$$

On the right-hand side of the above equation, the first term accounts for the short-range interaction, while the long-range interaction is described by the second term. In our calculation, the standard parametrization ($\alpha = 0.190$, $\beta = 0.460$, and $\mu = 0.330$) was used for both CAM-B3LYP and TD-CAM-B3LYP functionals. The CAM-B3LYP functional comprises of 0.19 Hartree–Fock (HF) plus 0.81 Becke 1988 (B88) exchange interaction at short-range, and 0.65 HF plus 0.35 B88 at long-range [27,28]. These range-separated functionals rely on a growing fraction of exact exchange when the interelectronic distance increases, subsequently providing a more physically sound model for long-range phenomena. It has been shown that the CAM-B3LYP functional proved efficient in the determination of the charge-transfer transition [29–35]. Furthermore, the CAM-B3LYP with $\alpha = 0.190$ and $\alpha + \beta = 0.65$ predictions of charge transfer excitations are in excellent agreement with the CASPT2 results [27]. Therefore, the geometries of **1**–**10** in the ground states (S_0) and the first excited singlet state (S_1) have been optimized by using the CAM-B3LYP and TD-CAM-B3LYP functionals, respectively. All geometry optimizations were performed using the 6-31G(d,p) basis set. The harmonic vibrational frequency calculations using the same methods as for the geometry optimizations were used to ascertain the presence of a local minimum. Absorption and fluorescent properties of **1**–**10** have been predicted using the TD-B3LYP/6-31+G(d,p) method based on the S_0 and S_1 optimized geometries, respectively. The atomic charges in S_0 and S_1 were calculated by the natural population analysis (NPA) [36], using the built-in NBO-3.1 subroutines of the Gaussian.

3. Results and discussion

3.1. Geometry optimization

The optimized structures of **1**–**10** in S_0 are shown in Fig. 2. A summary of the important inter-ring bond lengths and dihedral angles in S_0 and S_1 is given in Table 1. The Cartesian coordinates of **1**–**10** for the S_0 and S_1 are given in Supplementary Tables SI and SII, respectively. In the S_0, the comparison of the optimization results for three fragments TPA, CB, and NI of investigated molecules does not reveal any significant change in the geometry of the skeleton. The main structural changes occurred between the adjacent fragments. For **1**, the inter-ring distances TPA–CB and CB–NI are 1.458 and 1.382 Å, respectively. The inter-ring dihedral angles TPA–CB and CB–NI are 5.6 and 23.8°, respectively. For **2**–**10**, the inter-ring distances TPA–CB and CB–NI increase from 1.453 to 1.480 Å and from 1.467 to 1.486 Å, respectively. The inter-ring dihedral angles TPA–CB and CB–NI increase from 5.6° to 46° and from 33.1° to 60.1°, respectively. Both the inter-ring bond lengths and dihedral angles of **2**–**10** in S_0 increase compared with those of **1**, which is due to the steric hindrances. Furthermore, the dihedral angle between two thiophen rings in CB for **10** is −24.1°, suggesting that the conjugative effect between TPA, CB, and NI fragments is weaker than that of other D–π–A bipolar molecules.

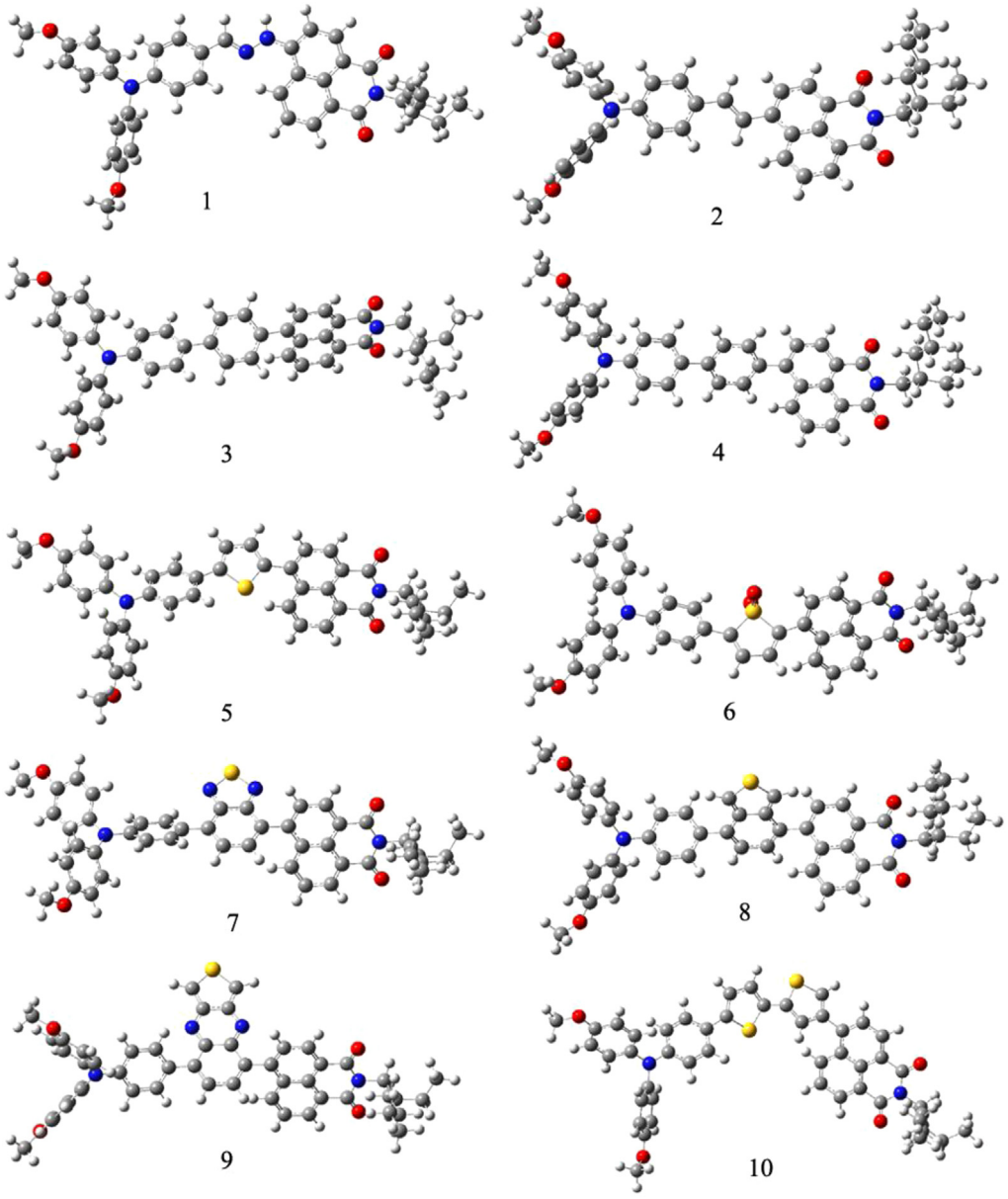

Fig. 2. The stereograph of optimized compounds **1**–**10** at the CAM-B3LYP/6-31G(d,p) level.

Table 1
Optimized important inter-ring distances (D) and dihedral angles (θ) of **1**–**10** in the S_0 and S_1 at the CAM-B3LYP/6-31G(d,p) and TD-CAM-B3LYP/6-31G(d,p) levels, respectively.

Species	S_0				S_1			
	D (Å)		θ (deg)		D (Å)		θ (deg)	
	TPA[a]–CB[b]	CB–NI[c]	TPA–CB	CB–NI	TPA–CB	CB–NI	TPA–CB	CB–NI
1	1.458	1.382	5.6	23.8	1.419	1.373	1.3	3.0
2	1.462	1.467	−5.6	−33.1	1.422	1.417	0.4	0.9
3	1.480	1.485	36.7	53.7	1.445	1.443	18.7	33.8
4	1.480	1.485	35.8	−56.0	1.444	1.442	19.2	−33.3
5	1.466	1.474	29.2	48.2	1.423	1.427	3.1	22.5
6	1.453	1.466	21.4	45.7	1.421	1.427	5.3	27.9
7	1.475	1.483	35.1	55.4	1.448	1.458	11.3	39.4
8	1.480	1.486	46.0	−60.1	1.444	1.444	30.8	−39.9
9	1.480	1.486	−42.0	59.7	1.455	1.474	−28.9	49.6
10	1.465	1.480	28.7	54.2	1.410	1.479	0.9	49.3

[a] TPA: triphenylamine fragments.
[b] CB: conjugated bridge fragments.
[c] NI: 1,8-naphthalimide fragments.

Electronic excitation leads to the large varieties of the bipolar molecules structures as shown in Table 1. Both the inter-ring bond lengths and dihedral angles of **2**–**10** in S_1 increase compared with those of **1** except the corresponding dihedral angles of **2** are similar to that of **1**, which is also due to the steric hindrances. The inter-ring bond lengths are shortened and the dihedral angles become smaller compared with those in S_0. For example, the inter-ring distances TPA–CB and CB–NI of **3** reduce from 1.480 to 1.445 Å and from 1.485 to 1.443 Å, respectively. The inter-ring dihedral angles TPA–CB and CB–NI of **3** reduce from 36.7° to 18.7° and from 53.7° to 33.8°, respectively. Similar phenomena are also found for other bipolar molecules. Moreover, the dihedral angle between two thiophen rings in π-conjugated bridge for **10** is almost 0°, suggesting that the conjugative effect between TPA, CB, and NI fragments is stronger than that in S_0. This implies that the singlet excited structures between the two adjacent fragments in the bipolar molecules should be more planar than their ground structures for investigated molecules. It suggests that the TPA, CB, and NI fragments have strong conjugative effect in S_1. As a consequence, the electron can flow easily from electron-donating moieties to the electron-withdrawing fragments, resulting in the large bathochromic shifts in their absorption and fluorescence spectra.

3.2. Frontier molecular orbitals and natural population analysis

It is useful to examine the frontier molecular orbitals (FMOs) of the compounds under investigation. The origin of the geometric difference introduced by excitation can be explained, at least in qualitative terms, by analyzing the change in the bonding character of the orbitals involved in the electronic transition for each pair of bonded atoms [37]. An electronic excitation results in some electron density redistribution that affects the molecular geometry [37,38]. To characterize the optical transitions and the abilities of electron and hole transport, we calculated the distribution patterns of FMOs for **1**–**10** in S_0 (see Fig. 3). The corresponding HOMO−1 and LUMO+1 of **10** in S_0 are given in Supplementary Fig. SI. The total and partial densities of states (TDOS and PDOS) on each fragment of the investigated molecules around the HOMO–LUMO gaps were calculated based on the current level of theory. The results are plotted for **1**–**10** shown in Supplementary Fig. SII. The FMOs energies E_{HOMO} and E_{LUMO}, HOMO–LUMO gaps E_g, and HOMOs and LUMOs contributions of individual fragments (in %) to the FMOs of **1**–**10** are given in Table 2. As shown in Fig. 3, the $S_0 \rightarrow S_1$ excitation process can be mainly assigned to the HOMO → LUMO transition, which corresponds to a π–π^* excited singlet state. For all molecules, the HOMOs are mainly composed of contributions of the TPA and CB fragments, with minor contributions from NI fragments. The sum contributions of TPA and CB fragments are larger than 87%, while the corresponding contributions of NI fragments are within 13%. However, the LUMOs of **1**–**10** are mainly distributed on the atoms of the NI fragments except for **7** and **9**. The contributions of NI fragments are larger than 82% except for **6**, **7,** and **9** (55.7% for **6**, 30.8% for **7**, and 0.6% for **9**). Interestingly, the LUMOs of **7** and **9** are mainly localized at the atoms of the CB fragments (64.4% for **7** and 96.0% for **9**), with minor contributions from TPA and NI fragments. Furthermore, the HOMO−1 and LUMO+1 of **10** are distributed mainly on the atoms of the CB and TPA fragments (96.1% for HOMO−1 and 97.8% for LUMO+1), with minor contributions from NI fragments (see detail discussion and Fig. SI in Supplementary).

The distribution patterns of the HOMOs and LUMOs also provide a remarkable signature for the charge-transfer character of the vertical $S_0 \rightarrow S_1$ transition. Analysis of the FMOs for **1**–**10** indicates that the excitation of the electron from the HOMO to LUMO leads the electronic density to flow mainly from the TPA and CB fragments to NI fragments for **1**–**5**, **8**, and **10** and from the TPA fragments to NI and CB fragments for **6**, **7**, and **9**, respectively. The percentages of charge transfer from TPA and CB fragments to NI fragments for **1**–**5**, **8**, and **10** decrease in the order of **10** (95.1%) > **3** (94.0%) > **4** (93.9%) > **5** (91.1%) > **8** (90.4%) > **2** (81.0%) > **1** (80.0%). The percentages of charge transfer from TPA fragments to NI and CB fragments for **6**, **7**, and **9** are in the sequence **9** (98.2%) > **7** (95.4%) > **6** (92.9%). Furthermore, the excitations of HOMO → LUMO+1 and HOMO−1 → LUMO for **10** lead the electronic density to flow mainly from TPA fragment to NI and CB fragments (64.7%) and from TPA and CB fragments to NI fragment (89.4%), respectively (see detail discussion and Fig. SI in Supplementary). The results displayed in Table 2 reveal that the TPA and NI fragments save as donors and acceptors for the compounds under investigation, respectively. However, the CB fragments save as donors for **1**–**5**, **8**, and **10** and as acceptors for **6**, **7**, and **9**, respectively.

The overall NPA charge transfer has been evaluated by summing up the NPA atomic charges on the TPA, CB, and NI fragments of each compound. The calculated NPA charge densities are collected in Table 3. It clearly shows that the values of Δq on TPA fragments are positive, while the corresponding values of Δq on NI fragments are negative for the compounds under investigation. A positive value of Δq indicates that the TPA fragment is electron-donating in nature; on the other hand, a negative value implies the electron-withdrawing nature of the NI fragment. Thus, one may conclude that the TPA and NI fragments save as donors and acceptors for the compounds under investigation, respectively. However, the values of Δq on CB fragments for **1**–**5**, **8**, and **10** are positive, while the corresponding values of **6**, **7**, and **9** are negative. It suggests that the CB fragments save as donors for **1**–**5**, **8**, and **10** and as acceptors for **6**, **7**, and **9**, respectively. Furthermore, from the Δq values of CB fragments, one can find that the electron-donating abilities of CB fragments decrease in the following order: **5** > **1** > **2** > **8** > **3** > **4** > **10** and the electron-withdrawing abilities of CB fragments are in the sequence **6** > **9** > **7**. Hence, the charge-transfer character of the vertical $S_0 \rightarrow S_1$ transition and the properties of donors/acceptors are also supported by NPA analysis. Furthermore, the photophysical properties of ICT are well known and highly dependent on the electron donor/acceptor strength [39,40]. The introduction of π-conjugated bridges strengthens the electron-donating (-withdrawing) abilities of donors (acceptors). Therefore, the ICT transition in the D–π–A bipolar molecules becomes much easier after introducing of π-conjugated bridges, resulting in the large bathochromic shift in their absorption and fluorescence spectra.

From Table 2, one can find that the E_{HOMO} values of **2**–**10** are similar to that of **1** except the corresponding value of **6** decreases compared with that of **1**. However, both the E_{LUMO} and E_g values of **2**–**10** decrease compared with those of **1**.

3.3. Charge transport properties and stability properties

The charge transfer rate can be described by Marcus theory [41,42] via the following equation:

$$K = \left(\frac{V^2}{\hbar}\right)\left(\frac{\pi}{\lambda k_B T}\right)^{1/2} \exp\left(\frac{-\lambda}{4k_B T}\right)$$

where T is the temperature, k_B is the Boltzmann constant, λ represents the reorganization energy due to geometric relaxation accompanying charge transfer, and V is the electronic coupling matrix element (transfer integral) between the two adjacent species dictated largely by orbital overlap. It is clear that two key parameters are the reorganization energy and electronic coupling matrix element, which have a dominant impact on the charge transfer rate, especially the former. In this paper, we focus on their reorganization energies λ to investigate their charge transport properties. Generally, the λ can be divided into two parts, external

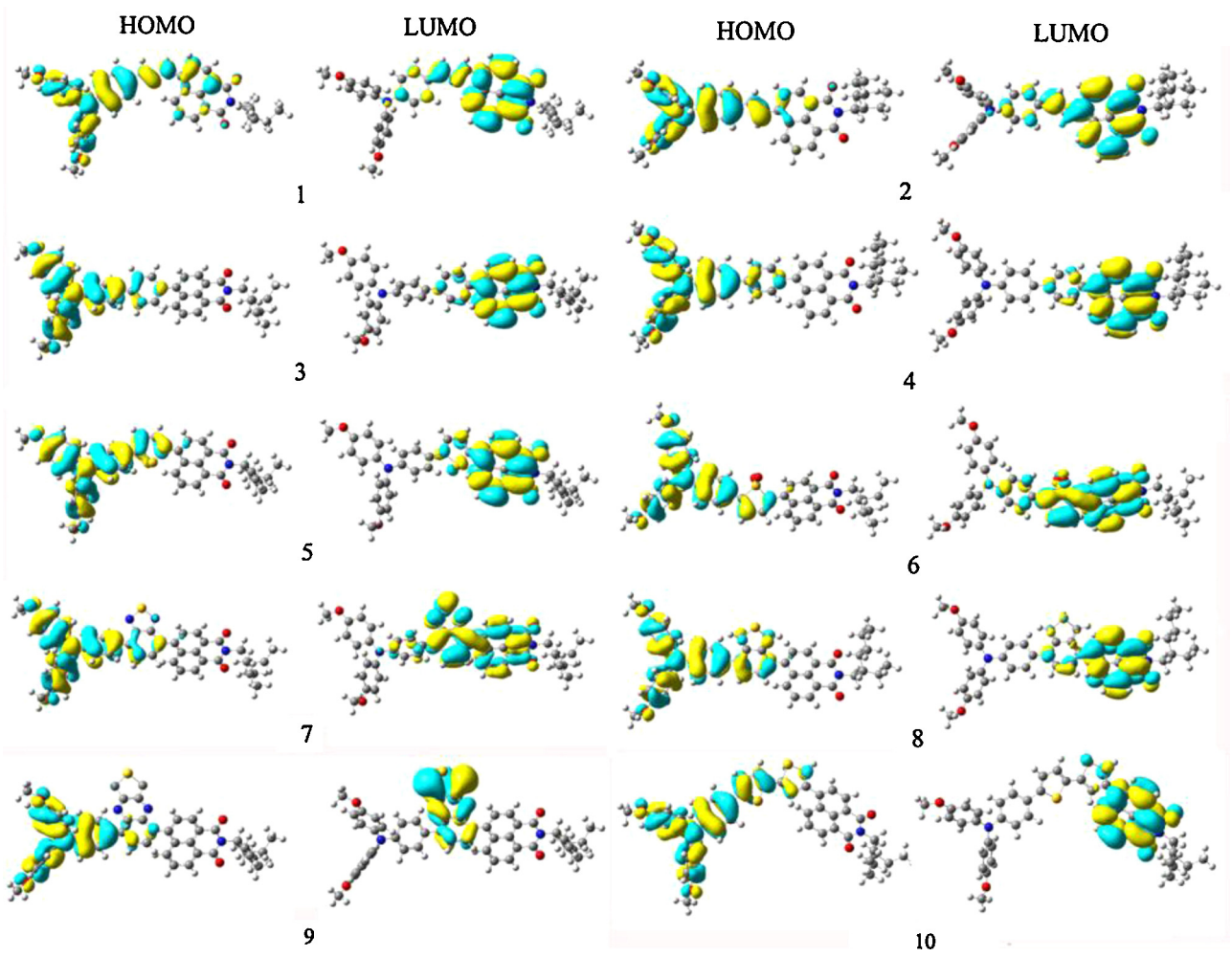

Fig. 3. Electronic density contours of the frontier orbitals for compounds **1**–**10** (blue and yellow refer to the different phases of molecular wave functions, and the isovalue is 0.02 a.u.).

reorganization energy (λ_{ext}) and internal reorganization energy (λ_{int}). λ_{ext} represents the effect of polarized medium on charge transfer; on the other hand, λ_{int} is a measure of structural change between ionic and neutral states [43,44]. Our designed molecules are used as charge transport materials for OLEDs in the solid film; the dielectric constant of the medium for the molecules is low. The computed values of the external reorganization energy in pure organic condensed phases are not only small but also are much smaller than their internal counterparts [45–47]. Moreover, there is a clear correlation between λ_{int} and charge transfer rate in literature [48,49]. The reorganization energy could be an important factor that governs the mobility of charge carriers [50]. Therefore, we only pay attention to the discussion of the λ_{int} of the isolated active organic systems due to ignoring any environmental relaxation and changes in this paper. Our calculations of the reorganization energy associated with different geometries of two states

Table 2
The HOMO and LUMO energies (E_{HOMO} and E_{LUMO}, in eV), HOMO–LUMO gaps (E_g, in eV), and HOMOs and LUMOs contributions of individual fragments (in %) to HOMOs and LUMOs of **1**–**10** at the CAM-B3LYP/6-31G(d,p) level.

Species	HOMO				LUMO				
	E_{HOMO}	NI[a]	CB[b]	TPA[c]	E_{LUMO}	NI[a]	CB[b]	TPA[c]	E_g
1	−6.03	12.7	14.1	73.2	−0.89	82.7	10.1	7.2	5.14
2	−6.04	5.9	9.0	85.1	−1.20	86.9	6.8	6.3	4.84
3	−6.02	0.8	5.2	94.0	−1.13	94.8	4.4	0.8	4.89
4	−6.02	0.7	5.2	94.1	−1.14	94.6	4.6	0.8	4.89
5	−6.02	1.4	9.6	89.0	−1.20	92.5	6.4	1.1	4.82
6	−6.22	1.5	8.4	90.0	−1.59	55.7	37.2	7.1	4.63
7	−6.06	1.0	7.0	92.0	−1.40	30.8	64.4	4.6	4.66
8	−6.01	1.1	11.9	86.9	−1.16	91.5	7.7	0.8	4.86
9	−5.98	0.7	6.7	92.6	−1.80	2.1	96.0	1.8	4.18
10	−5.95	0.1	16.2	83.6	−1.18	95.3	4.7	0.0	4.78

[a] TPA: triphenylamine fragments.
[b] CB: conjugated bridge fragments.
[c] NI: 1,8-naphthalimide fragments.

Table 3
The natural population analysis (NPA) for **1**–**10** in the S_0 and S_1 at the CAM-B3LYP/6-31G(d,p) and TD-CAM-B3LYP/6-31G(d,p) levels, respectively.

Species	q (S_0)			q (S_1)			Δq[d]		
	NI[c]	CB[b]	TPA[a]	NI	CB	TPA	NI	CB	TPA
1	0.037	−0.063	0.026	0.013	−0.049	0.036	−0.024	0.014	0.010
2	−0.064	0.034	0.030	−0.101	0.044	0.057	−0.037	0.010	0.027
3	−0.022	−0.002	0.024	−0.048	0.002	0.046	−0.026	0.004	0.022
4	−0.022	−0.002	0.024	−0.048	0.001	0.047	−0.026	0.003	0.023
5	−0.026	−0.002	0.028	−0.083	0.033	0.050	−0.057	0.035	0.022
6	0.004	−0.095	0.091	−0.025	−0.113	0.138	−0.029	−0.018	0.047
7	−0.002	−0.057	0.059	−0.020	−0.066	0.086	−0.018	−0.009	0.027
8	−0.021	−0.004	0.025	−0.051	0.003	0.048	−0.030	0.007	0.023
9	−0.006	−0.038	0.044	−0.018	−0.049	0.067	−0.012	−0.011	0.023
10	−0.011	−0.016	0.027	−0.013	−0.015	0.028	−0.004	0.001	0.001

[a] TPA: triphenylamine fragments.
[b] CB: conjugated bridge fragments.
[c] NI: 1,8-naphthalimide fragments.
[d] $\Delta q = q(S_1) - q(S_0)$.

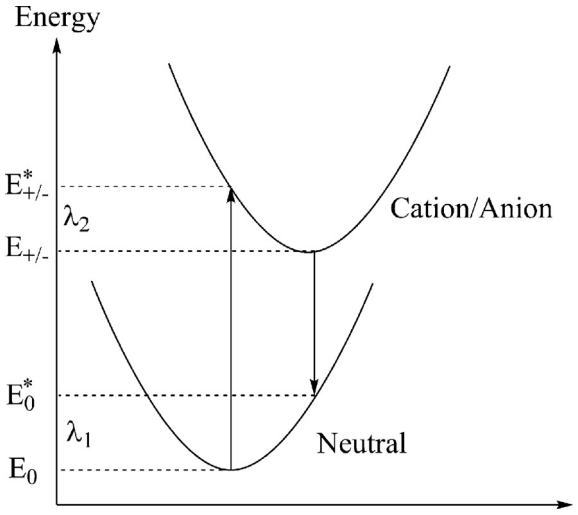

Fig. 4. Sketch of the potential energies of neutral and cation/anion species, illustrating the neutral (λ_1) and cation/anion (λ_2) relaxation energies.

are based on the hopping model schematically illustrated in Fig. 4. For comparing with the interested results reported previously [51,52], the reorganization energies for electron (λ_e) and hole (λ_h) of the molecules were predicted from the single point energy at the B3LYP/6-31G(d,p) level based on the CAM-B3LYP/6-31G(d,p) optimized neutral, cationic, and anionic geometries.

The calculated reorganization energies for hole and electron are listed in Table 4. It is well-known that, the lower the reorganization energy values, the higher the charge transfer rate [41,42]. The results displayed in Table 4 show that the calculated λ_h values of **1**–**10** (0.232–0.264 eV) except for **6** are much smaller than that of N,N′-diphenyl-N,N′-bis(3-methylphenyl)-(1,1′-biphenyl)-4,4′-diamine (TPD), which is a typical hole transport material (λ_h = 0.290 eV) [52]. The λ_h value of **6** (0.293) is similar to that of TPD. It indicates that their hole transfer rates may be higher than that of TPD. It suggests that **1**–**10** could be good electron transfer materials from the stand point of the λ_h values. On the other hand, the λ_e values of **1**–**10** (0.326–0.657 eV) are larger than that of tris(8-hydroxyquinolinato)aluminum(III) (Alq3) (λ_e = 0.276 eV), a typical electron transport material [51]. It implies that the electron transfer rates of **1**–**10** might be lower than that of Alq3. Inspection of Table 4 reveals clearly that the both λ_h and λ_e values of these bipolar molecules are similar to those of **1** except the corresponding values of **6** (λ_h = 0.293 eV, λ_e = 0.657 eV) are slightly larger than those of **1**. It suggests that different π-conjugated bridges do not significantly affect both the λ_h and λ_e values. It indicates that **1**–**10** can be used as promising hole transport materials in OLEDs from the stand point of the smaller reorganization energy.

Table 4
The calculated reorganization energies for electron (λ_e) and hole (λ_h) of the molecules and the absolute hardness (η) of the molecules (all in eV) for **1**–**10** at the B3LYP/6-31G(d,p)//CAM- B3LYP/6-31G(d,p) level.

Species	λ_h	λ_e	η
1	0.259	0.449	2.365
2	0.232	0.543	2.261
3	0.254	0.410	2.358
4	0.255	0.415	2.354
5	0.260	0.517	2.251
6	0.293	0.657	2.071
7	0.263	0.510	2.133
8	0.239	0.445	2.259
9	0.240	0.385	1.990
10	0.264	0.326	2.273

As the stability is a useful criterion to evaluate the nature of devices for charge transport and luminescent materials. To predict the stability of **1**–**10** from a viewpoint of molecular orbital theory, the absolute hardness, η, of **1**–**10** were calculated using operational definitions [53,54] given by:

$$\eta = \frac{1}{2}\left(\frac{\partial \mu}{\partial N}\right) = \frac{1}{2}\left(\frac{\partial^2 E}{\partial N^2}\right) = \frac{IP - EA}{2}$$

where μ is the chemical potential and N is the total electron number. In this work, the values for IP (adiabatic ionization potential) and EA (adiabatic electron affinity) were determined according to the equation $IP = E_{cr} - E_p$ and $EA = E_p - E_{ar}$, where p, cr, and ar indicate the parent molecule and the corresponding cation and anion radical generated after electron transfer.

The absolute hardness η is the resistance of the chemical potential to change in the number of electrons. As expected, inspection of Table 4 reveals clearly that **2**–**10** have nearly equal values of absolute hardness, being smaller slightly than the value of **1**. It indicates that the stabilities of **2**–**10** are smaller slightly than that of **1**, which may be due to the steric hindrances. These results reveal that the different π-conjugated bridges do not significantly affect the stability of these bipolar molecules.

3.4. Absorption and fluorescence spectra

The absorption λ_{abs} and fluorescence λ_{fl} wavelengths, the oscillator strength f, and main assignments of **1**–**10** are listed in Tables 5 and 6, respectively. The λ_{abs} and λ_{fl} values of **1** are all in agreement with experimental results [24], the deviations are 6

Table 5
The absorption wavelengths λ_{abs} (in nm), the oscillator strength *f*, and main assignments (coefficient) of **1**–**10** at the TD-B3LYP/6-31+G(d,p)//CAM-B3LYP/6-31G(d,p) level, along with available experimental data.

Species	λ_{abs}	*f*	Main assignment	Exp[a]
1	504	0.66	H[b] → L[c] (98%)	511
2	551	0.53	H → L (100%)	
3	558	0.12	H → L (100%)	
4	560	0.11	H → L (100%)	
5	580	0.14	H → L (98%)	
6	601	0.57	H → L (98%)	
7	614	0.33	H → L (98%)	
8	572	0.13	H → L (98%)	
9	806	0.12	H → L (98%)	
10	435	0.67	H → L+1 (65%) H − 1 → L (34%)	

[a] Experimental data were taken from Ref. [24].
[b] H: HOMO.
[c] L: LUMO.

and 18 nm, respectively. This reveals that the level of theory we selected is reasonable for this kind of system.

To investigate the influence of solvents on the optical properties for the S_0 and S_1 states of the molecular systems in tetrahydrofuran (THF, dielectric constant: 7.43) and toluene (dielectric constant: 2.37) solvents, we selected the parent compound (**1**) as representative of the system under investigation and performed the polarized continuum model (PCM) [55] calculations at the TD-DFT level. The λ_{abs} and λ_{fl} of **1** in THF and toluene solvents are given in Supplementary Table SIII. From Table SIII, one can find that the λ_{abs} value of **1** in gas phase is in agreement with experimental result measured as thin films [24], the deviation is only 7 nm. However, the λ_{abs} value of **1** in THF solvent shows larger deviation from experimental data (the deviation is 77 nm) than that in gas phase. The λ_{fl} values of **1** both in THF and toluene solvents also show larger deviations from experimental data than those in gas phase, the deviations are 37 and 64 nm, respectively. The discrepancy may be ascribed to the defect of PCM [56,57]. Furthermore, our designed molecules are used as charge transport and luminescent materials for OLEDs in the solid film. Therefore, the solvent effect for investigated system is negligible in this work.

The absorption of **1**–**9** are assigned to the $S_0 \rightarrow S_1$ electronic transitions and HOMOs → LUMOs excitations play a dominant role. From Table 5, one can find that the λ_{abs} of **2**–**9** have strong bathochromic shifts compared with that of the parent compound **1**, the deviations are 47, 54, 56, 76, 97, 110, 68, and 202 nm, respectively. The fluorescence of **1**–**9** are assigned to the $S_0 \leftarrow S_1$ electronic transitions and LUMOs ← HOMOs excitations play a dominant role. As shown in Table 6, the λ_{fl} values of **2**–**9** show bathochromic shifts 43, 54, 76, 44, 145, 161, 76 and 388 nm, respectively.

Table 6
The fluorescence wavelengths λ_{flu} (in nm), the oscillator strength *f*, and main assignments (coefficient) of **1**–**10** at the TD-B3LYP/6-31 + G(d,p)//TD-CAM-B3LYP/6-31(d,p) level, along with available experimental data.

Species	λ_{flu}	*f*	Assignment	Exp[a]
1	561	0.96	H[b] ← L[c] (98%)	543
2	604	1.05	H ← L (98%)	
3	615	0.56	H ← L (100%)	
4	617	0.58	H ← L (100%)	
5	637	0.87	H ← L (98%)	
6	706	1.15	H ← L (100%)	
7	722	0.62	H ← L (98%)	
8	637	0.74	H ← L (98%)	
9	949	0.21	H ← L (98%)	
10	527	1.19	H ← L+1 (98%)	

[a] Experimental data in toluene were taken from Ref. [24].
[b] H: HOMO.
[c] L: LUMO.

Interestingly, the absorption of **10** is assigned to the $S_0 \rightarrow S_2$ electronic transition and the HOMOs → LUMOs+1 excitation plays a dominant role. The fluorescence of **10** is assigned to the $S_0 \leftarrow S_2$ electronic transition and LUMO ← HOMO+1 excitation plays a dominant role. The λ_{fl} and λ_{fl}, the oscillator strength *f*, and main assignments (coefficient) corresponding to $S_0 \rightarrow S_1$ and $S_0 \leftarrow S_1$ electronic transitions respectively of **10** are listed in Supplementary Table SIV. As shown in Tables 5 and 6, the λ_{abs} value of **10** shows strong hypsochromic shift (the deviation is 69 nm), while the corresponding value of λ_{fl} shows slightly hypsochromic shift (34 nm) compared with that of **1**. As mentioned above, this can be explained by the fact that the **10** has worse conjugation due to large twist angle between two thiophen rings in π-conjugated bridge (−24.1°) in S_0. It suggests that the conjugative effect between TPA, CB, and NI fragments in **10** becomes lower than that in **1**, resulting in the large hypsochromic shift between their UV–vis spectra. However, the twist angle between two thiophen rings in π-conjugated bridge in S_1 become almost 0°, suggesting that the conjugative effect between TPA, CB, and NI fragments is stronger than that in S_0. Therefore, the λ_{fl} value of **10** shows slightly hypsochromic shift (34 nm) compared with that of **1**.

Moreover, from Table 5, we can find that **1**, **2**, **6**, and **10** have much larger oscillator strengths than those of other compounds. The oscillator strength for an electronic transition is proportional to the transition moment [58]. In general, larger oscillator strength corresponds to larger experimental absorption coefficient or stronger fluorescence intensity. This indicates that **1**, **2**, **6**, and **10** shown larger absorption intensity than those of other compounds. On the other hand, from Table 6, we also find that the *f* values of **3**–**5** and **7**–**9** are slightly less than that of **1**. The *f* values of **2**, **6**, and **10** are larger than that of **1**, corresponding to strong fluorescence spectra. This implies that these bipolar molecules have large fluorescent intensity and they are useful as fluorescent OLED materials, particularly for **1**, **2**, **6**, and **10**. The reason may be the low inter-ring dihedral angles TPA–CB and/or CB–NI of **1**, **2**, **6**, and **10** both in S_0 and S_1 (see Table 1), suggesting that the TPA, CB, and NI fragments have strong conjugative effects, resulting in the large absorption and fluorescent intensity.

As shown in Tables 5 and 6, the absorption and fluorescence spectra of this series of bipolar molecules exhibit bathochromic shifts to some extent due to the electron-withdrawing/donating properties of the π-conjugated bridges. It clearly shows that all the π-conjugated bridge can significantly affect the fluorescence spectra of these bipolar molecules. Furthermore, **2**, **6**, and **10** show the most intensive absorption and fluorescence spectra among the bipolar molecules.

4. Conclusions

In this paper, a series of bipolar molecules, which have the same donor (triphenylamine moiety) and acceptor (1,8-naphthalimide moiety) as well as different π-conjugated bridge, has been systematically investigated. The geometries of compounds in the ground states and the first excited singlet state have been optimized by using the CAM-B3LYP and TD-CAM-B3LYP functionals, respectively. The FMOs, NPA, and local density of states analysis have turned out that the vertical electronic transitions of absorption and emission are characterized as intramolecular charge transfer (ICT). The calculated results show that their optical and electronic properties are affected by the π-conjugated bridges of the bipolar molecules. The electron-donating (withdrawing) π-conjugated bridges serve as donors (acceptors) for the compounds under investigation. Our results suggest that **1**–**10** are expected to be promising candidates for hole transport and luminescent materials for OLEDs. On the basis of investigated results, we proposed a rational way

for the design of charge transport and/or luminescent materials simultaneously.

Acknowledgement

Financial support from the Natural Science Foundation of Inner Mongolia Autonomous Region (no. 2011ZD02) is gratefully acknowledged.

Appendix A. Supplementary data

Supplementary data associated with this article can be found, in the online version, at http://dx.doi.org/10.1016/j.jmgm.2013.04.001.

References

[1] S. Miyata, H.S. Nalwa, Organic Electroluminescent Materials and Devices, Gordon and Breach, New York, 1997.
[2] K. Müllen, U. Scherf, Organic Light-emitting Devices, Synthesis, Properties, and Applications, Wiley-VCH, Weinheim, 2006.
[3] K. Walzer, B. Maennig, M. Pfeiffer, K. Leo, Highly efficient organic devices based on electrically doped transport layers, Chemical Reviews 107 (2007) 1233–1271.
[4] A.C. Grimsdale, K.L. Chan, R.E. Martin, P.G. Jokisz, A.B. Holmes, Synthesis of light-emitting conjugated polymers for applications in electroluminescent devices, Chemical Reviews 109 (2009) 897–1091.
[5] H.E. Katz, Z.N. Bao, S.L. Gilat, Synthetic chemistry for ultrapure, processable, and high-mobility organic transistor semiconductors, Accounts of Chemical Research 34 (2001) 359–369.
[6] C.D. Dimitrakopoulos, P.R.L. Malenfant, Organic thin film transistors for large area electronics, Advanced Materials 14 (2002) 99–117.
[7] P. Peumans, A. Yakimov, S.R. Forrest, Small molecular weight organic thin-film photodetectors and solar cells, Journal of Applied Physics 93 (2003) 3693–3723.
[8] A. Kraft, A.C. Grimsdale, A.B. Holmes, Electroluminescent conjugated polymers–seeing polymers in a new light, Angewandte Chemie International Edition 37 (1998) 402–428.
[9] Z. He, W.Y. Wong, X. Yu, H.S. Kwork, Z. Lin, Phosphorescent platinum(II) complexes derived from multifunctional chromophores: synthesis, structures, photophysics, and electroluminescence, Inorganic Chemistry 45 (2006) 10922–10937.
[10] J. Slinker, D. Bernards, P.L. Houston, H.D. Abruña, S. Bernhard, G.G. Malliaras, Solid-state electroluminescent devices based on transition metal complexes, Chemical Communications 19 (2003) 2392–2399.
[11] Y.L. Liu, J.K. Feng, A.M. Ren, Theoretical study on photophysical properties of bis-dipolar diphenylamino-endcapped oligoarylfluorenes as light-emitting materials, Journal of Physical Chemistry A 112 (2008) 3157–3164.
[12] L.Y. Zou, A.M. Ren, J.K. Feng, Y.L. Liu, X.Q. Ran, C.C. Sun, Theoretical study on photophysical properties of multifunctional electroluminescent molecules with different π-conjugated bridges, Journal of Physical Chemistry A 112 (2008) 12172–12178.
[13] S. Tang, J. Zhang, Rational design of organic asymmetric donors D1–A–D2 possessing broad absorption regions and suitable frontier molecular orbitals to match typical acceptors toward solar cells, Journal of Physical Chemistry A 115 (2011) 5184–5191.
[14] A. Kukhta, E. Kolesnik, I. Grabchev, S. Sali, Spectral and luminescent properties and electroluminescence of polyvinylcarbazole with 1,8-naphthalimide in the side chain, Journal of Fluorescence 16 (2006) 375–378.
[15] J. Liu, J.X. Cao, S.Y. Shao, Z.Y. Xie, Y.X. Cheng, Y.H. Geng, L.X. Wang, X.B. Jing, F.S. Wang, Blue electroluminescent polymers with dopant-host systems and molecular dispersion features: polyfluorene as the deep blue host and 1,8-naphthalimide derivative units as the light blue dopants, Journal of Materials Chemistry 18 (2008) 1659–1666.
[16] C.Y. Mei, G.L. Tu, Q.G. Zhou, Y.X. Cheng, Z.Y. Xie, D.G. Ma, Y.H. Geng, L.X. Wang, Green electroluminescent polyfluorenes containing 1,8-naphthalimide moieties as color tuner, Polymer 47 (2006) 4976–4984.
[17] S. Wang, P.J. Zeng, Y.Q. Liu, G. Yu, X.B. Sun, H.B. Niu, D.B. Zhu, Luminescent properties of a novel naphthalimide-fluorene molecule, Synthetic Metals 150 (2005) 33–38.
[18] H. Tian, J.H. Su, K.C. Chen, T.C. Wong, Z.Q. Gao, C.S. Lee, S.T. Lee, Electroluminescent property and charge separation state of bis-naphthalimides, Optical Materials 14 (2000) 91–94.
[19] F. Cacialli, R.H. Friend, C.M. Bouche, P. Le Barny, H. Facoetti, F. Soyer, P. Robin, Naphthalimide side-chain polymers for organic light-emitting diodes: band-offset engineering and role of polymer thickness, Journal of Applied Physics 83 (1998) 2343–2356.
[20] W. Zhu, M. Hu, Y. Wu, H. Tian, R.G. Sun, A.J. Epstein, Novel luminescent carbazole-naphthalimide dyads for single-layer electroluminescent device, Synthetic Metals 119 (2001) 547–548.
[21] J.L. Hua, B. Li, F.S. Meng, F. Ding, S.X. Qian, H. Tian, Two-photon absorption properties of hyperbranched conjugated polymers with triphenylamine as the core, Polymer 45 (2004) 7143–7149.
[22] L. Janis, F.H. John, Discrete high molecular weight triarylamine dendrimers prepared by palladium-catalyzed amination, Journal of the American Chemical Society 119 (1997) 11695–11696.
[23] Y. Kuwabara, H. Ogawa, H. Inada, N. Noma, Y. Shirota, Thermally stable multilayered organic electroluminescent devices using novel starburst molecules, 4,4′,4″-Tri(N-carbazolyl)triphenylamine (TCTA) and 4,4′,4″-Tris(3-methylphenylphenylamino)triphenylamine (m-MTDATA), as hole-transport materials, Advanced Materials 6 (1994) 677–679.
[24] D. Gudeika, R. Lygaitis, V. Mimaitė, J.V. Grazulevicius, V. Jankauskas, M. Lapkowski, P. Data, Hydrazones containing electron-accepting and electron-donating moieties, Dyes and Pigments 91 (2011) 13–19.
[25] M.J.T. Frisch, G.W. Trucks, H.B. Schlegel, G.E. Scuseria, M.A. Robb, J.R. Cheeseman, G. Scalmani, V. Barone, B. Mennucci, G.A. Petersson, H. Nakatsuji, M. Caricato, X. Li, H.P. Hratchian, A.F. Izmaylov, J. Bloino, G. Zheng, J.L. Sonnenberg, M. Hada, M. Ehara, K. Toyota, R. Fukuda, J. Hasegawa, M. Ishida, T. Nakajima, Y. Honda, O. Kitao, H. Nakai, T. Vreven, J.A. Montgomery Jr., J.E. Peralta, F. Ogliaro, M. Bearpark, J.J. Heyd, E. Brothers, K.N. Kudin, V.N. Staroverov, R. Kobayashi, J. Normand, K. Raghavachari, A. Rendell, J.C. Burant, S.S. Iyengar, J. Tomasi, M. Cossi, N. Rega, J.M. Millam, M. Klene, J.E. Knox, J.B. Cross, V. Bakken, C. Adamo, J. Jaramillo, R. Gomperts, R.E. Stratmann, O. Yazyev, A.J. Austin, R. Cammi, C. Pomelli, J.W. Ochterski, R.L. Martin, K. Morokuma, V.G. Zakrzewski, G.A. Voth, P. Salvador, J.J. Dannenberg, S. Dapprich, A.D. Daniels, O. Farkas, J.B. Foresman, J.V. Ortiz, J. Cioslowski, D.J. Fox, Gaussian 09, Gaussian, Inc., Wallingford, CT, USA, 2009.
[26] N.C. Handy, The molecular physics lecture 2004: (i) Density functional theory, (ii) Quantum monte carlo, Molecular Physics 102 (2004) 2399–2499.
[27] Y. Tawada, T. Tsuneda, S. Yanagisawa, T. Yanai, K. Hirao, A long-range-corrected time-dependent density functional theory, Journal of Chemical Physics 120 (2004) 8425–8433.
[28] T. Yanai, D.P. Tew, N.C. Handy, A new hybrid exchange—correlation functional using the coulomb-attenuating method (CAM-B3LYP), Chemical Physics Letters 393 (2004) 51–57.
[29] V. Hrobáriková, P. Hrobárik, P. Gajdoš, I. Fitilis, M. Fakis, P. Persephonis, P. Zahradník, Benzothiazole-based fluorophores of donor–π–acceptor–π–donor type displaying high two-photon absorption, Journal of Organic Chemistry 75 (2010) 3053–3068.
[30] P. Hrobárik, V. Hrobáriková, I. Sigmundová, P. Zahradník, M. Fakis, I. Polyzos, P. Persephonis, Benzothiazoles with tunable electron-withdrawing strength and reverse polarity: a route to triphenylamine-based chromophores with enhanced two-photon absorption, Journal of Organic Chemistry 76 (2011) 8726–8736.
[31] P. Hrobárik, I. Sigmundová, P. Zahradník, P. Kasák, V. Arion, E. Franz, K. Clays, Molecular engineering of benzothiazolium salts with large quadratic hyperpolarizabilities: can auxiliary electron-withdrawing groups enhance nonlinear optical responses? Journal of Physical Chemistry C 114 (2010) 22289–22302.
[32] R. Kobayashi, R.D. Amos, The application of CAM-B3LYP to the charge-transfer band problem of the zincbacteriochlorin–bacteriochlorin complex, Chemical Physics Letters 420 (2006) 106–109.
[33] I.S.K. Kerkines, I.D. Petsalakis, G. Theodorakopoulos, Excited-state intramolecular proton transfer in hydroxyoxime-based chemical sensors, Journal of Physical Chemistry A 115 (2011) 834–840.
[34] I.V. Rostov, R.D. Amos, R. Kobayashi, G. Scalmani, M.J. Frisch, Studies of the ground and excited-state surfaces of the retinal chromophore using CAM-B3LYP, Journal of Physical Chemistry B 114 (2010) 5547–5555.
[35] X. Liu, X. Zhang, Y. Hou, F. Teng, Z. Lou, Theoretical investigation on properties of the ground and lowest excited states of a red emitter with donor–π–acceptor structure, Chemical Physics 381 (2011) 100–104.
[36] A.E. Reed, L.A. Curtiss, F. Weinhold, Intermolecular interactions from a natural bond orbital, donor–acceptor viewpoint, Chemical Reviews 88 (1988) 899–926.
[37] M. Forés, M. Duran, M. Solà, L. Adamowicz, Excited-state intramolecular proton transfer and rotamerism of 2-(2′-hydroxyvinyl)benzimidazole and 2-(2′-hydroxyphenyl)imidazole, Journal of Physical Chemistry A 103 (1999) 4413–4420.
[38] A. Helal, M.H.O. Rashid, C.H. Choi, H.S. Kim, Chromogenic and fluorogenic sensing of Cu^{2+} based on coumarin, Tetrahedron 67 (2011) 2794–2802.
[39] Z. Wen, Y. Jiang, Ratiometric dual fluorescent receptors for anions under intramolecular charge transfer mechanism, Tetrahedron 60 (2004) 11109–11115.
[40] W. Huang, X. Zhang, L. Ma, C. Wang, Y. Jiang, Intramolecular charge transfer dual fluorescence of substituted-phenyl *p*-dimethylaminobenzoates with comparable electron acceptors, Chemical Physics Letters 352 (2002) 401–407.
[41] R.A. Marcus, Electron transfer reactions in chemistry. Theory and experiment, Reviews of Modern Physics 65 (1993) 599–610.
[42] R.A. Marcus, Chemical and electrochemical electron-transfer theory, Annual Review of Physical Chemistry 15 (1964) 155–196.
[43] V. Lemaur, M. Steel, D. Beljonne, J.L. Brédas, J. Cornil, Photoinduced charge generation and recombination dynamics in model donor/acceptor pairs for organic solar cell applications: a full quantum-chemical treatment, Journal of the American Chemical Society 127 (2005) 6076–6077.
[44] G.R. Hutchison, M.A. Ratner, T.J. Marks, Hopping transport in conductive heterocyclic oligomers: reorganization energies and substituent effects, Journal of the American Chemical Society 127 (2005) 2339–2350.

[45] D.L. Cheung, A. Troisi, Theoretical study of the organic photovoltaic electron acceptor PCBM: morphology, electronic structure, and charge localization, Journal of Physical Chemistry C 114 (2010) 20479–20488.
[46] N.G. Martinelli, J. Idé, R.S. Sánchez-Carrera, V. Coropceanu, J.L. Brédas, L. Ducasse, F. Castet, J. Cornil, D. Beljonne, Influence of structural dynamics on polarization energies in anthracene single crystals, Journal of Physical Chemistry C 114 (2010) 20678–20685.
[47] D.P. McMahon, A. Trois, Evaluation of the external reorganization energy of polyacenes, Journal of Physical Chemistry Letters 1 (2010) 941–946.
[48] M.E. Köse, H. Long, K. Kim, P. Graf, D. Ginley, Charge transport simulations in conjugated dendrimers, Journal of Physical Chemistry A 114 (2010) 4388–4393.
[49] K. Sakanoue, M. Motoda, M. Sugimoto, S. Sakaki, A molecular orbital study on the hole transport property of organic amine compounds, Journal of Physical Chemistry A 103 (1999) 5551–5556.
[50] Y.A. Berlin, G.R. Hutchison, P. Rempala, M.A. Ratner, J. Michl, Charge hopping in molecular wires as a sequence of electron-transfer reactions, Journal of Physical Chemistry A 107 (2003) 3970–3980.
[51] B.C. Lin, C.P. Cheng, Z.Q. You, C.P. Hsu, Charge transport properties of tris(8-hydroxyquinolinato)aluminum(III): why it is an electron transporter, Journal of the American Chemical Society 127 (2005) 66–67.
[52] N.E. Gruhn, D.A. da Silva Filho, T.G. Bill, M. Malagoli, V. Coropceanu, A. Kahn, J.L. Brédas, The vibrational reorganization energy in pentacene: molecular influences on charge transport, Journal of the American Chemical Society 124 (2002) 7918–7919.
[53] R.G. Pearson, Absolute electronegativity and absolute hardness of Lewis acids and bases, Journal of the American Chemical Society 107 (1985) 6801–6806.
[54] M.S. Start, Epoxidation of alkenes by peroxyl radicals in the gas phase: structure–activity relationships, Journal of Physical Chemistry A 101 (1997) 8296–8301.
[55] J.P. Cornard, C. Lapouge, Absorption spectra of caffeic acid, caffeate and their 1:1 complex with Al(III): density functional theory and time-dependent density functional theory investigations, Journal of Physical Chemistry A 110 (2006) 7159–7166.
[56] C.J. Cramer, D.G. Truhlar, Reply to comment on “a universal approach to solvation modeling”, Accounts of Chemical Research 42 (2009) 493–497.
[57] S. Meng, J. Ma, Solvatochromic shift of donor–acceptor substituted bithiophene in solvents of different polarity: quantum chemical and molecular dynamics simulations, Journal of Physical Chemistry B 112 (2008) 4313–4322.
[58] P. von Ragué Schleyer, N.L. Allinger, T. Clark, J. Gasteiger, P.A. Kollman, H.F. Schaefer III, P.R. Schreiners, Encyclopedia of Computational Chemistry, Wiley, Chichester, UK, 1998, pp. 2646–2664.